Available online at www.sciencedirect.com
SCIENCE DIRECT®

Computers and Structures 82 (2004) 2211–2219

Computers & Structures

www.elsevier.com/locate/compstruc

Ship shock modeling and simulation for far-field underwater explosion

Young S. Shin *

Department of Mechanical Engineering, Naval Postgraduate School, Monterey, CA 93943, USA

Received 25 November 2002; accepted 24 March 2004

Abstract

Surface ship shock trials have been conducted in many countries for shock qualification of ship integrity, systems and subsystems. The ship shock trial identifies design and construction deficiencies that have a negative impact on ship and crew survivability. It also validates shock hardening criteria and performance. However, ship shock trials are costly. As a possible alternative, numerical modeling and simulation may provide viable information to look into the details of dynamic characteristics of ship including component and sub-component level. Ship shock analyses were conducted using finite element based coupled ship and fluid model. Three-dimensional ship shock modeling and simulation has been performed and the predicted results were compared with ship shock test data. Surface ship shock analysis approach is presented and the important parameters are discussed.
Published by Elsevier Ltd. and Civil-Comp Ltd.

Keywords: Underwater explosion; Ship shock; Modeling; Simulation

1. Introduction

Surface ship shock simulation subjected to underwater explosion is generally complicated by free surface effects such as surface reflection wave resulting bulk cavitation. In addition, hull cavitation, gas bubble oscillation and migration toward free surface, and cavitation closure pulses. Furthermore, there are complex fluid–structure interaction phenomena, and the dynamic behavior of the ship, shipboard systems and sub-systems. The underwater shock response of a two-dimensional mid-section model of surface ship was predicted with a coupled surrounding fluid model [1]. Recently, three-dimensional ship shock analyses were conducted using a large scale finite element model of a coupled ship and surrounding fluid [2]. This paper addresses a three-dimensional analysis of a surface ship finite element model coupled with a surrounding fluid model subjected to a far-field underwater explosion. LS-DYNA code [3,4] coupled with USA code [5–7] was used to conduct the ship shock analysis.

2. Free field problem—loading mechanisms

The loading mechanisms due to underwater explosion include incident shock wave, free surface reflection wave, bottom reflection wave, gas bubble oscillation and bubble-pulse loading, and bulk and hull cavitations. The shock wave referred here is pressure wave.

* Tel.: +1 831 656 2568; fax: +1 831 656 2238.
E-mail address: yshin@nps.navy.mil

0045-7949/$ - see front matter Published by Elsevier Ltd. and Civil-Comp Ltd.
doi:10.1016/j.compstruc.2004.03.075

2.1. Underwater explosion

The explosion is defined as chemical reaction in a substance which converts the original material into a gas at very high temperature and pressure [8]. It is a self-oxidized process and generates gaseous products. Explosives do not usually have high energy contents of ordinary fuels. However, the rate of energy release during the detonation process results in greater destructive power.

From the standpoint of the ship design against the underwater explosion, the water media may be assumed as homogeneous fluid with no shear stress capabilities and acoustic wave propagating velocity of 4900 ft/s at 18 °C. The types of wave form considered here is a spherical shock wave. For the spherical wave, the amplitude decays as it propagates in radial direction. The pressure wave in the reacting explosive begins outward motion of the water. The underwater shock wave pressure decreases exponentially and lasts a few milliseconds. The shock wave has a steep front.

The pressure wave really determines the nature of the explosion. It begins in one section of the explosive and, as it propagates through the explosive, it initiates the chemical reaction which, in turn, emits more pressure waves. Therefore, once the explosion is initiated in one section of the explosive, it tends to propagate itself through the explosive. However, the process is not explained that simply. The pressure wave may be altered by release waves which propagate in from the explosive boundary and by various explosive characteristics. The increase in pressure results in increased wave velocity until the wave velocity exceeds the speed of sound in the explosive. A shock wave is thus found in the explosive. The shock wave pressure behind the shock front along with the high temperature change combines to initiate the explosive reaction. Hence, the detonation becomes a self-exerted process which proceeds at a steady rate.

The are two fundamental classification of explosives; pure explosives (or primary explosive) and explosive mixtures (or high explosive). A pure explosive is a chemically unstable substances which decomposes under the action of extremely applied influences. Thus decomposition consists of a complete rupture of the intermolecular bonds. It consists of a single chemical substances throughout the body. A explosive mixture consists of mixtures of different chemical substances. The application of external excitation results in a chemical reaction between the various substances. Generally one substance is oxygen rich but this is not always the case. Explosive mixtures may be gaseous, liquid, or combination. The full names of explosives, for examples, are Cyclotrimethylenetrinitramine (RDX), Trinitrotouluene (TNT), and Trinitrophenylmethylnitramine (TETRYL). The pure explosive is very sensitive, has rather low detonation speed and low power generated compared with high explosive. The shock wave propagation velocity near the charge is 3–5 times of acoustic speed in the water, 5000 ft/s. The shock wave profile is inversely proportional to the distance. The shock wave propagation velocity converges rapidly to acoustic wave velocity in the distance of about ten charge radius. Therefore, the ship shock analysis is valid when the standoff distance is at least ten charge radius. The linear/acoustic considerations are valid for ship shock analysis in this range.

Approximately half of the total energy is initially contained in the gas sphere and the gas pressure is much higher than the atmospheric plus hydrostatic pressure. As a result, the gas bubble expands radially with a large outward velocity. The expansion does not stop even if gas pressure equalizes with the atmospheric plus hydrostatic pressure because of the inertia effect of the water surrounding the gas sphere. When the bubble reaches to its maximum, it starts to contract with an increasing inward velocity because of the pressure difference at the bubble boundary. The compressibility of gas limits the further contraction of gas bubble and reverses it motion rapidly. When the bubble is minimum in size, it collapses and generates the bubble pulse. The bubble oscillation continues until gas energy is dissipated all into the water or venting out into the air at the free surface. The effect of gravity generally causes the gas bubble to migrate upward while it oscillates. The gas bubble motion, shock pressure and the gas bubble shapes are shown in Fig. 1. As can be seen in Fig. 1, the bubble rises

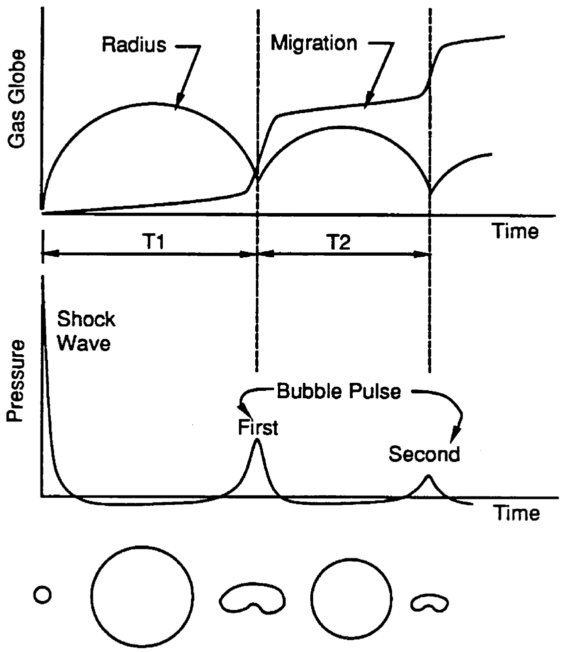

Fig. 1. Gas bubble growth, migration and bubble pulse.

faster when the bubble size is minimum. It is caused by the fact that the drag due to the hydrodynamic mass surrounding the gas sphere is minimum. The simple dynamic law, "linear impulse is the change in momentum" explains the reasoning well [9]. The resulting expression shows

$$U(t) = -\frac{2g}{a^3(t)} \int_0^t a^3(x)\,dx \tag{1}$$

where $U(t)$ is vertical velocity of gas bubble, $a(t)$ is radius of gas bubble, g is gravitational acceleration and negative sign(–) implies upward direction toward free surface. As the above equation shows, the gas bubble velocity, $U(t)$ is inversely proportional to the third power of bubble radius, resulting faster bubble rise when the bubble is in minimum size. When the incident shock wave hits the free surface, the spray dome appears. Subsequently, white plumes burst into the air due to the bubble pulses. Finally, black plume caused by gaseous product appears and concludes the sequence of underwater explosion events.

2.2. Shock wave parameters

An explosive detonated underwater exerts high explosive pressure on the surrounding water. Although water is considered incompressible under usual conditions, there is a considerable unit volume change. The water is compressed and attains a high radial velocity. Since the water is compressible in this case the disturbance will propagate roughly at the acoustic velocity in water. This velocity, of course, depends on the magnitude of the pressure, temperature and density. Corrections can be made for these parameters. For all discussions in this paper, in general, the wave propagation rate will be taken as the acoustic velocity in water. The value of the acoustic speed is usually taken as 5000 ft/s. This disturbance travelling radially at the acoustic velocity is referred to as the shock wave. The characteristic of shock wave near the explosive is not very well known. The relations become increasingly uncertain near the surface of the charge, owing to the lack of knowledge of the equation of state. Since this paper will not cover contact explosions, only the characteristic of the shock wave at some distance is needed here [9].

The shock formulas presented here are fairly accurate at distances between 10 and 100 charge radii, and for a duration up to one decay constant in time. The empirically determined equation of the pressure profile has the following form:

$$P(t) = P_{\max} e^{-\frac{t-t_1}{\theta}} \quad t \geqslant t_1 \tag{2}$$

where t is the time elapsed after the detonation of charge in ms, t_1 is the arrival time of shock wave to the target after the detonation of charge in ms, $P_{\max}$ is the peak pressure magnitude (psi) in the shock wave front and θ is the decay constant which describes the exponential decay in ms. This approximation is only good, however, for pressure greater than about one third of the peak value.

$$P_{\max} = K_1 \left(\frac{W^{\frac{1}{3}}}{R}\right)^{A_1} \quad (\text{psi}) \tag{3}$$

$$\theta = K_2 W^{\frac{1}{3}} \left(\frac{W^{\frac{1}{3}}}{R}\right)^{A_2} \quad (\text{psi}) \tag{4}$$

where K_1, A_1, K_2, A_2 are constants which depend on explosive types and are shown.

2.3. Gas bubble behavior and bubble-pulse loading

The chemical reaction produces gases at very high temperatures and pressures. At very early times the gas pressure acts on the surrounding water resulting in compression and radial motion of the water. Thus the shock wave is produced and emitted. About half of the energy of the explosion is emitted in the shock wave. During the formation of the shock wave, the gas pressure is much higher than the hydrostatic pressure. As the shock wave passes each water particle, the water particle attains a radial velocity. This motion of the water particle behind the shock front is essentially incompressible flow where the pressure in the water drops at or below hydrostatic pressure. Thus it is reasonable to use incompressible flow theory to describe gas bubble motion and behaviour in general.

As long as the gas pressure in the bubble is greater than the hydrostatic pressure and the radial flow of the water is outward, the gas is doing the work on the water and thus using up its own internal energy. At some time in the motion, the pressure of the internal bubble gas reaches the point of equilibrium with hydrostatic pressure. But at the time the flow is still radially outward and thus the gas pressure begins to drop below hydrostatic pressure. The internal energy of the gas at this time is small and essentially negligible. This point of equilibrium is reached when the bubble radius is less than half of the maximum radius that it will eventually reach. At this low pressure, it is reasonable to apply the incompressible flow equations to determine the behaviour [8].

Following the time of maximum radius, the hydrostatic pressure reverses the radial flow and the eventually collapses producing a pressure pulse. The pressure pulse causes radial flow and the cycle repeats until the total bubble energy is emitted. When the bubble contracts to the minimum in size, compressible flow equations are more appropriate to determine the dynamic behaviour. The empirical expressions for first explosion gas bubble period (T) and maximum radius ($A_{\max}$) are

Table 1
Shock wave parameter values

Description	Parameter	Explosive type		
		HBX-1	TNT	PETN
P_{max} (Max. pressure)	K_1	22,347	22,505	24,589
	A_1	1.144	1.18	1.194
Decay constants	K_2	0.056	0.058	0.052
	A_2	−0.247	−0.185	−0.257
Bubble period	K_5	4.761	4.268	4.339
Bubble radius	K_6	14.14	12.67	12.88

$$T = K_5 \frac{W^{\frac{1}{3}}}{(D+33)^{\frac{5}{6}}} \text{ (s)} \quad (5)$$

$$A_{max} = K_6 \frac{W^{\frac{1}{3}}}{(D+33)^{\frac{1}{3}}} \text{ (s)} \quad (6)$$

where T is a gas bubble period in s. and D is a charge depth in feet. K_5, K_6 are constants shown in Table 1.

The gas bubble composes about 47% of the explosive energy and the bubble pulse pressure can cause damage just as the shock wave can. The buoyancy and bubble migration effects can result in the bubble collapse occurring close to a target. In the shallow depth of water, the gas pressure is less than even atmospheric pressure when the bubble radius is near the maximum. It is apparent what will happen if the depth of the explosion is less than, but near the maximum size of bubble. As the bubble reaches the surface, air at atmospheric pressure rushes in the cavity which is at a much lower pressure. The hydrostatic pressure will now have to compress the vented air in order to close the cavity. The air acts as a cushion allowing the closure and virtually eliminates any closure pressure pulse. It should be obvious that bubble venting requires that the explosion depth be less than the maximum bubble radius. Experience indicates that results would be satisfactory if the depth is between 50% and 80% of the maximum radius.

2.4. Bulk cavitation

Cavitation is a phenomenon which occurs in water caused by the reflection of a shock wave at a free surface. When the region which cavitates is large, it is called "Bulk Cavitation." A simple description would be that the compression shock wave reflecting from a free surface results in a tensile reflected wave (rarefaction wave). Since the water cannot sustain a significant amount of tension, cavitation occurs in the water and the surrounding pressure rises to the vapor pressure of water (about 0.3 psi). The cavitated region forms the bulk cavitation envelope which has the upper and lower boundaries. The water behind the shock front at the time of cavitation, has a velocity depending on the location relative to the charge and the surface. The water near the surface, for example, has primarily a vertical velocity at the time of cavitation. After the passage of the reflected shock wave the water particles are acted on by gravity or gravity and atmospheric pressure. Methods to compute bulk cavitation can be found in the references [10,11].

3. Fluid–structure interaction

3.1. Doubly asymptotic approximation

The underwater-shock fluid–structure interaction problem is based on doubly asymptotic approximation (DAA) [12,13]. The DAA approach models the acoustic medium surrounding the structure as a membrane covering the wet surface of the structure. The principal advantage of the DAA is that it models the interaction of the submerged structure with the surrounding acoustic medium in terms of wet-surface response variables only, eliminating the need for fluid volume elements around the outside of the structure. The DAA may be used to determine the fluid pressure generated by the scattered wave on the wet surface of the structure. The governing equation of motion for the structure and the DAA equation with the interface compatibility relation is used to solve the dynamic response of the system.

The discretized differential equation for the structure can be expressed as

$$M_s\ddot{x}(t) + C_s\dot{x}(t) + K_s x(t) = f(t) \quad (7)$$

where $x(t)$ is the structural displacement vector, M_s, C_s and K_s are mass, damping and stiffness matrices, respectively, $f(t)$ is the external force vector and a dot denotes a temporal derivative. For excitation of a submerged structure by an acoustic wave, $f(t)$ is given by

$$f(t) = -GA_f[p_i(t) + p_s(t)] + f_d(t) \quad (8)$$

where $p_i(t)$ and $p_s(t)$ are nodal incident(known) and scattered(unknown) wave pressure vectors for the wet-surface fluid mesh, respectively, $f_d(t)$ is the applied force vector for the dry-structure, A_f is the diagonal area matrix converting nodal pressures to nodal forces and G is the transformation matrix associated with fluid and structural nodal surface forces.

The first-order doubly asymptotic approximation can be expressed as [12,13]

$$M_f\dot{p}_s(t) + \rho c A_f p_s(t) = \rho c M_f \dot{u}_s(t) \tag{9}$$

where M_f is the fluid mass matrix for the wet-surface fluid mesh, ρ and c are the density and acoustic velocity of the fluid, respectively, and $u_s(t)$ is the vector of scattered-wave fluid particle velocities normal to the structure's wet surface. The DAA equation (9) is called 'doubly asymptotic' because it exhibits the correct asymptotic behavior in both the high-frequency (early-time) and low-frequency (late-time) limits. For high-frequency motion, $|\dot{p}_s(t)|$ term is significantly higher than $|p_s(t)|$, so that the second term in the left-hand side of Eq. (9) is negligible compared with the first term resulting in the plane wave approximation, $p_s(t) = \rho c u_s(t)$ which is accurate for sufficiently short acoustic wavelengths. For low-frequency motion, $|p_s(t)|$ term is significantly higher than $|\dot{p}_s(t)|$, and Eq. (9) approaches the virtual mass approximation $A_f p_s(t) = M_f \dot{u}_s(t)$ which is accurate for sufficiently long acoustic wavelengths.

The fluid–structure interface compatibility relation can be expressed as

$$G^T\dot{x} = u_i + u_s \tag{10}$$

where the superscript 'T' denotes matrix transposition. Eq. (10) expresses the fluid particle velocity and the structural velocity normal to the set-surface of the structure are equal at the interface.

Substituting Eq. (8) into Eq. (7), Eq. (10) into Eq. (9), and assuming $f_d(t)$ is zero,

$$M_s\ddot{x} + C_s\dot{x} + K_s x = -GA_f[p_i(t) + p_s(t)] \tag{11}$$

$$M_f\ddot{p}_s(t) + \rho c A_f p_s(t) = \rho c M_f[G^T\ddot{x}(t) - \dot{u}_i] \tag{12}$$

Eqs. (11) and (12) can be solved simultaneously at each time step for x and p_s. The improved second-order DAA is available [13]. Again DAA approach is excellent approximation technique to eliminate the need for modeling surrounding fluid volume, and covering the wet surface of the structure with DAA boundary elements.

3.2. Cavitating fluid model

When the shock wave impinges on ship hull and if the hull kick-off velocity is higher than the adjacent fluid particle velocity, local cavitation phenomenon occurs in the fluid in addition to the bulk cavitation phenomenon near the free surface. Subsequently, the cavitated region closes. The effective mathematical model for this phenomenon was formulated and discussed in Ref. [7]. It treats wave propagation for small irrotational compressible motions with bilinear constitutive behavior for cavitating fluid. In this case the first-order DAA equation serves as a radiation boundary where the fluid volume is truncated.

4. LS-DYNA and USA codes

The finite element code used for dynamic response analysis of ship structure is LS-DYNA (nonlinear dynamic analysis of structures in three dimensions) [3,4]. This explicit integration based code has been widely used for a variety of nonlinear engineering problems since its introduction in 1976. Its wide array of material models, equations of state and many distinct features results in a high degree of versatility [3]. This code is also accessible to many users in that it is operational on PCs, workstations and mainframe computers.

The surrounding fluid is modeled using solid volume elements with MAT_90 (MAT_ACOUSTIC) material property in LS-DYNA code. This model is capable of treating wave propagation for small irrotational compressible motions with either linear or bilinear constitutive behavior for non-cavitating or cavitating fluids. This bilinear fluid cannot transmit negative total pressure and acoustic fluid volume element has only a pressure degree-of-freedom [3,7]. The surrounding fluid volume is truncated and the first-order DAA [12,13] is placed at the truncated fluid volume as a radiation boundary.

The Underwater Shock Analysis (USA) code is a boundary element code for the underwater-shock fluid–structure interaction problem [5,6] based on doubly asymptotic approximation (DAA). The DAA approach models the acoustic medium surrounding the structure as a membrane covering the wet surface of the structure. The principal advantage of the DAA is that it models the interaction of the structure with the surrounding acoustic medium in terms of wet-surface response variables only, eliminating the need for fluid volume elements around the outside of the structure. This approach works well for the deeply submerged structure where the cavitation is not a problem. However, for the surface ship shock analysis, the bulk and hull cavitations are important phenomena to take into account. Therefore, as mentioned in the previous paragraph, the finite volume of surrounding fluid is modeled to capture the cavitations in the fluid and the first-order DAA is placed at the outer faces of fluid volume. The governing equation of motion for the structure and surrounding fluid, and DAA equation with the interface compatibility relation are used to solve the dynamic response of the system. The USA was coupled with LS-DYNA and called as LS-DYNA/USA code which can solve many different classes of underwater shock problems.

5. 3-D coupled ship and fluid model

One of three-dimensional finite element (FE) model of surface ship is shown in Fig. 2. It was developed by Gibbs & Cox, Inc. [14]. The FE model includes the details of ship structures. Major stiffeners are modeled in as beam elements. The structural material properties assumed to remain linear elastic throughout the process.

The surrounding fluid model was developed using "extrusion" technique using TrueGrid code [15]. The surrounding fluid modeling along the keel line is very complex since keel line changes from knife-edge bow configuration to almost flat geometry as it approaches to stern area of ship. The fluid mesh consists of 8-noded solid elements. LS-DYNA's Material Type 90 (acoustic pressure element) is used to model the pressure wave transmission properties of water [3]. The coupled FE model of the ship and fluid system is shown in Fig. 3. The ship draft is 20.7 ft. The size of outskirts of surrounding fluid model is 585 ft long, 140 ft wide and 75 ft deep. The fluid model depth is close to the bulk cavitation boundary. The studies on the fluid mesh truncation effect on the response of a floating vessel [16] indicates that the fluid volume considered in this coupled model is sufficient to provide good simulation results.

The coupled ship and fluid LS-DYNA model characteristics are as follows:

- number of grid points 174,635
- number of fluid grid points 139,664
- number of ship grid points 34,971
- number of thin shell elements 41,708
- number of beam elements 41,952
- number of lumped masses 116,879
- number of discrete springs and dampers 416
- number of rigid body constraint sets 179
- number of solid (fluid volume) elements 94,199
- number of DAA fluid boundary faces 4290

An important feature of the fluid mesh is the element size next to the ship mesh. The computational stability consideration leads to the following relation for the fluid element thickness in the direction normal to the wetted ship hull [7]:

$$\frac{2\rho D}{\rho_s t_s} \leqslant 5 \tag{13}$$

where ρ = density of water, D = thickness of the fluid element in the direction normal to the wetted surface of the structure, ρ_s = density of the submerged structure, and t_s = thickness of the submerged structure.

6. Damping representation

The Rayleigh damping representation is used for damping in ship structural system and is defined as

$$[C] = \alpha[M] + \beta[K] \tag{14}$$

where $[C]$, $[M]$ and $[K]$ are the damping, mass and stiffness matrices, respectively. The constants, α and β are the mass and stiffness proportional damping constants. Transforming $[C]$ with the modal frequencies and modal damping factors,

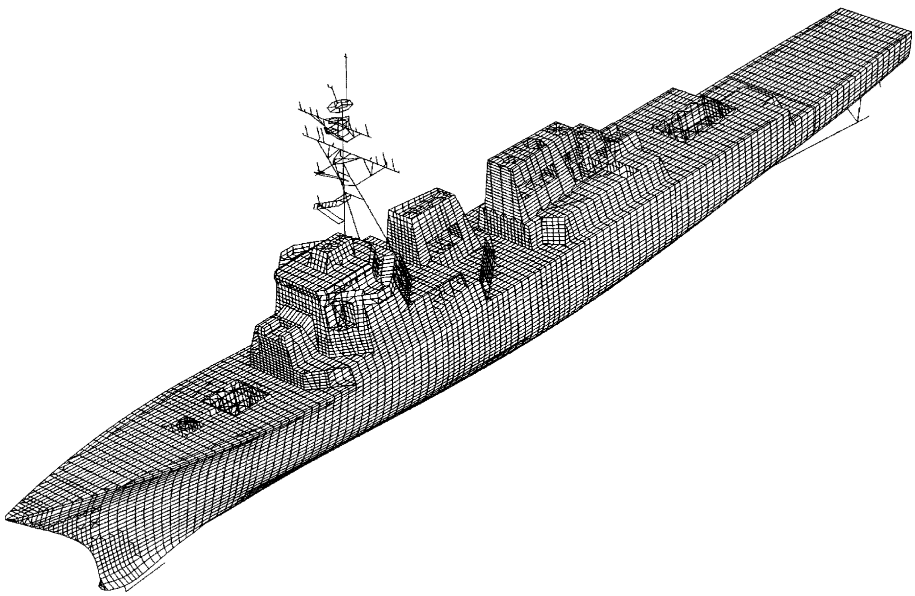

Fig. 2. Finite element model of surface ship [14].

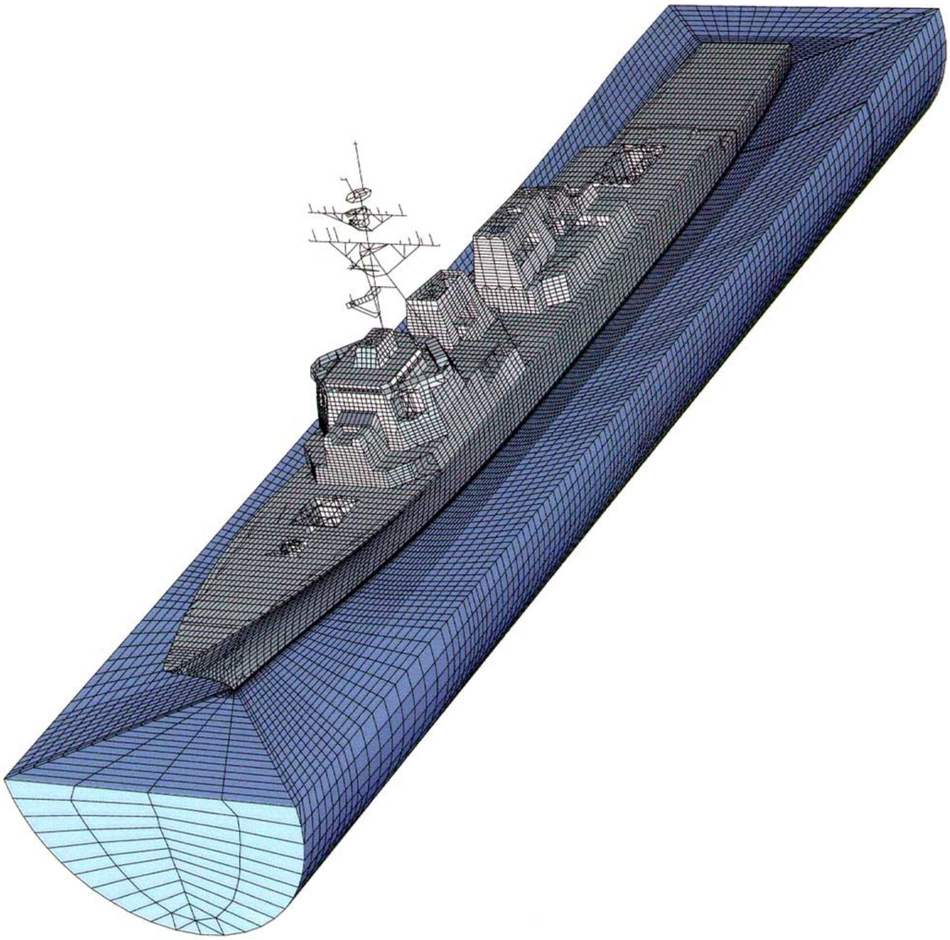

Fig. 3. Coupled finite element model of ship and surrounding fluid.

$$[2\zeta_i\omega_i] = \alpha[I] + \beta[\omega_i^2] \quad (15)$$

or for the ith mode,

$$2\zeta_i\omega_i = \alpha + \beta\omega_i^2 \quad (16)$$

where ζ_i and ω_i are ith modal damping factor and modal frequency, respectively. The constants, α and β may be determined from the past experimental ship test data.

7. Simulation results

The explosive charge is detonated in some distance away. The analysis results are compared with ship shock test data at various locations in keel and bulkhead. The computational time step size used is $4.0 \times 10^{**}(-6)$ s. The velocity responses in vertical direction are calculated and compared with ship shock test data. Figs. 4 and 5 show the vertical velocity response at the keel.

The predicted velocity responses compare well with the ship shock test data. Russell's error measure criteria

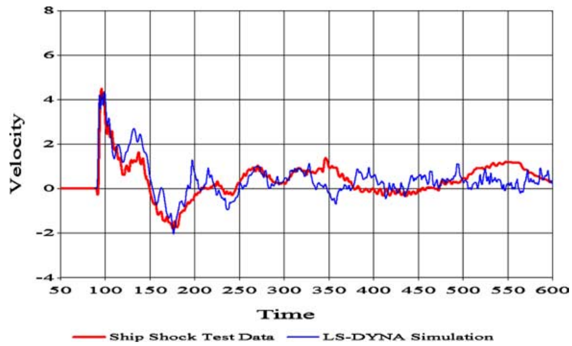

Fig. 4. Vertical response at keel—Case 1.

[17] was adapted to quantify how well a predicted ship shock response compares to a ship shock test data. It consists of Russell's Magnitude (RM), Phase (RP) and Comprehensive (RC) error factors. The Russell's error factors for Fig. 3 are RM = 0.025, RP = 0.2142 and

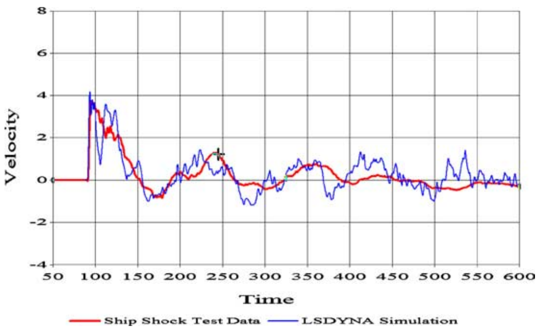

Fig. 5. Vertical response at keel—Case 2.

RC = 0.1911 which are well within acceptable limit. The small RM value, 0.025 indicates that the response magnitudes compares extremely well. The RP value of 0.2142 indicates that there exists some phase difference in the predicted and measured data, but still well within the acceptable limit. RC error factor is a composition of RM and RP values for overall error measure. Russell's error factors for Fig. 4 are RM = 0.088, RP = 0.2123 and RC = 0.2037 which are also well within acceptable limit.

Figs. 6 and 7 show the vertical velocity responses at the bulkhead, respectively. The predicted velocity responses in early time compare well with the ship shock test data. The phase does not correlate well in late time.

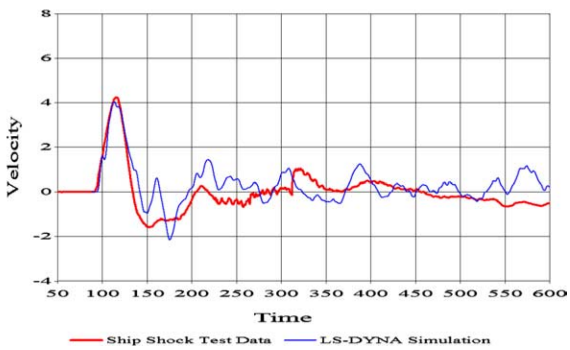

Fig. 6. Vertical velocity response at bulkhead—Case 3.

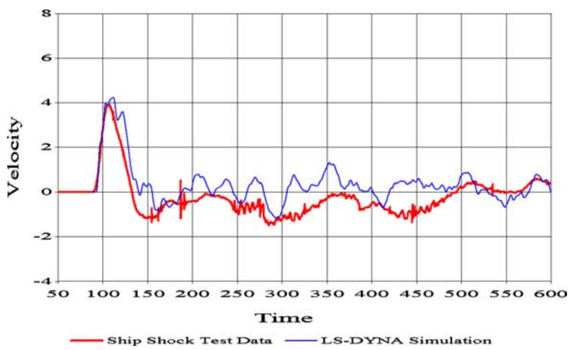

Fig. 7. Vertical velocity response at bulkhead—Case 4.

The Russell's error factors for Fig. 5 are RM = −0.0046, RP = 0.2465 and RC = 0.2185 which are within acceptable limit. The Russell's error factors for Fig. 6 are RM = 0.0363, RP = 0.2737 and RC = 0.2447 which are within acceptable limit.

8. Important parameters to be considered

For ship shock analysis in general, some considerations must be given to analysis issues: (a) type of analysis to perform, linear or nonlinear, Lagrangian, Eulerian, or coupled Lagrangian–Eulerian, (b) two-dimensional or three-dimensional analysis, (c) modeling techniques, (d) attack geometry, charge size and standoff distance, (e) ship whipping consideration, (f) gas bubble oscillation, (g) bulk and hull cavitation effect, (h) first- and second-order DAA, (i) material properties, etc. There are many more issues to be considered.

9. Summary and conclusion

Three-dimensional ship shock simulation is performed by modeling the coupled 3-D ship structures and surrounding fluid volume using the LS-DYNA/USA code. The simulation results are compared well with ship shock test data. The ship shock simulation conducted in this paper clearly demonstrates that three-dimensional full ship shock modeling and simulation can be achieved based on the state-of-the-art technologies and computer hardware.

Acknowledgments

The author extends his gratitude to CAPT David L. Lewis, USN, Mr. M. Winnette and Mr. C. Constant for their tireless discussions and encouragement throughout the course of ship shock modeling and simulation. I would also like to thank Dr. R. Rainsberger implementing "extrusion" technique in TrueGrid code to facilitate fluid modeling. I would also extend great thanks to all my research staffs and graduate students who dedicated in ship shock research. In addition, thanks are also due to Mr. T. Christian for his excellent job to make the computer always on-line.

References

[1] Shin YS, Santiago LD. Surface ship shock modelling and simulation: two-dimensional analysis. J Shock Vib 1998;5:129–37.

[2] Shin YS, Park SY. Ship shock trial simulation of USS John Paul Jones (DDG53) using LS-DYNA/USA: three dimensional analysis. Presented at 70th Shock and Vibration Symposium, Albuquerque NM, November 15–19, 1999.

[3] LSTC. LS-DYNA User's Manual: Nonlinear Dynamic Analysis of Structures in Three Dimensions, Version 940, Livermore Software Technology Corporation, Livermore, CA, June, 1997.
[4] Hallquist JO. LS-DYNA Theoretical Manual, Livermore Software Technology Corporation, Livermore, CA, May, 1998.
[5] DeRuntz Jr JA. The Underwater Shock Analysis (USA) Manual, Unique Software Applications, Colorado Spring, CO, May, 1996.
[6] DeRuntz Jr JA. The underwater shock analysis code and its application. Proc 60th Shock Vib Symp 1989;1: 89–107.
[7] DeRuntz Jr JA, Rankin CC. Applications of the USA-STAGS-CFA code to nonlinear fluid–structure interaction problems in underwater shock of submerged structures. Proc 60th Shock Vib Symp 1989;1:108–27.
[8] Cole RH. Underwater explosions. Princeton University Press; 1948.
[9] Shin YS, Geers TL. Response of marine structures to underwater explosion international short course lecture notes. Monterey, CA: Shock & Vibration Research; 1993.
[10] Arons AB, et al.. Long Range shock propagation in underwater explosion phenomena II. Underwater Explos Compend 1949;22:1.
[11] Costanzo FA, Gordon JD. An analysis of bulk cavitation in deep water. DTNSRDC, UERD Report, May, 1980.
[12] Geers TL. Residual potential and approximate methods for three-dimensional fluid–structure interaction problems. J Acoust Soc Am 1971;49(5):1505–10.
[13] Geers TL. Doubly asymptotic approximations for transient motions of submerged structures. J Acoust Soc Am 1978;64(5):1500–8.
[14] Gibbs & Cox, Inc. DDG53 full ship finite element documentation, Draft, May, 1998.
[15] XYZ Scientific Applications, Inc. TrueGrid User's Online Manual, Livermore, CA, 1998.
[16] Malone PE, Shin YS. Sensitivity analysis of coupled fluid volume to ship shock simulation. Proc 71st Shock Vib Symp 2000.
[17] Russell DM. Error measures for computing transient data: Part I: Development of a comprehensive error measure, Part II: Error measures case study. Proc 68th Shock Vib Symp 1997.